POST-DIGITAL - European Training Network on Post-Digital Computing [GA860360]

Document Details

Title	Deliverable 3.2 Report on final prototype of integrated neuromorphic system with integrated readout
Deliverable number	D3.2
Deliverable Type	Report (public)
Deliverable title	Report on final prototype of integrated neuromorphic system with integrated readout
Work Package	WP3 – Integrated Systems
Description	Document reporting results on integrated neuromorphic systems
Deliverable due date	30/09/2023
Actual date of submission	29/09/2023
Lead beneficiary	IMEC
Version number	V1.0
Status	Final

Dissemination level

PU	Public	X
CO	Confidential, only for members of the consortium (including Commission Services	

Project Details

Grant Agreement	860360
Project Acronym	POST-DIGITAL
Project Title	POST-DIGITAL - European Training Network on Post-Digital Computing
Call Identifier	H2020-MSCA-ITN-2019
Project Website	https://postdigital.astonphotonics.uk/
Start of the Project	1 April 2020
Project Duration	48 months

This project has received funding from the European Union's Horizon 2020 research and innovation programme under the Marie Skłodowska-Curie grant agreement No 860360.

EXECUTIVE SUMMARY

This deliverable describes the design of and results on several integrated neuromorphic systems done by ESRs at Ugent-imec, ULB, IBM, IFISC and VLC.

TABLE OF CONTENTS

Executive Summary 3
List of Figures 5
List of Acronyms 6
1 Introduction 7
2 Four-Port Reservoir Characterization and Experimental Results 7
2.1 Four-Port Reservoir Architecture 7
2.2 Readout Weights 8
2.2.1 Tungsten Heaters Weights 8
2.2.2 BTO Weights 10
2.3 Telecommunication Experiments 11
2.3.1 Intensity-Modulated (IM) and Direct Detected (DD) Signals 11
2.3.2 Coherently Modulated and Coherently Detected Signals 13
3 Characterization of Readout Layer for Frequency-Multiplexing Computers 14
3.1 Programmable Spectral Filter 15
3.1.1 Design 15
3.1.2 Characterization 16
3.2 Wavelength Converter 18
4 Photorefractive crossbar array 19
5 Characterization of Convolution Neural Network on Silicon Photonic Integrated Chip 20

LIST OF FIGURES

Figure 1 Design of a 4-node reservoir without an integrated readout....7
Figure 2 Design of a 4-node reservoir with integrated readout....8
Figure 3 Readout with weights....8
Figure 4 a. (left) Current drivers used to control readout weights b. (right) Wire-bonded chip placed on a PCB....9
Figure 5 Current vs output power for the pair of heaters of node 1....9
Figure 6 Dual driving of a pair of weights....10
Figure 7 a. (left) no modulation due to wrong polarization of light b. (right) optimized polarization hence modulation is seen....10
Figure 8 Modulation depths of 8 nodes on a reservoir chip....11
Figure 9 An 8-node reservoir with integrated BTO weights and summation tree....11
Figure 10 a. (left) data from tx-rx setup b. (right) data from tx-reservoir-rx setup....12
Figure 11 IM/DD system with a distorting optical fiber and a reservoir for equalization....12
Figure 12 a. (left) preliminary optimization to maximize transmission b. (right) optimization to minimize bit error rate....13
Figure 13 Coherent transmission setup....13
Figure 14 (a) Conceptual scheme of the programmable spectral filter. From left to right: 1-to-16 wavelength de-multiplexer, array of 16 attenuators, 16-to-1 multiplexer. (b) Detail of the de-multiplexer architecture. The de-multiplexer is composed of 15 lattice filters organized in a 4-stage binary three.....15
Figure 15 Experimental characterization setup. OSA: optical spectrum analyser; DUT: device under test.....16
Figure 16 (a) Cross-talk map of the spectral filter. The map reports the maximum extinction ratio measured on the “measured channel” when the “modulated channel” attenuation is swept. In-diagonal elements represent the actual extinction ratio of every channel, while the off-diagonal elements represent the cross-talk. The average cross-talk is 0.57 dB. (b) Measured transfer function for each of the 16 channels for different values of the driving current (in the range 0-5 mA). (c) Example of transmission function of a single channel....17
Figure 17 Scheme of the SOA-based wavelength converter. Both a frequency comb (blue arrow) and a low-power probe signal (λ_p, red arrow) are injected in the SOA. The SOA gain is saturated by the comb power and the saturation affects the gain experienced by the probe signal. A bandpass filter selects only the probe signal, whose power depends on the sum of the powers of the comb lines.....18
Figure 18 Envisioned application of the SOA-based wavelength converter. Note that the probe radiation power is lower than the comb power, hence the representations of the spectrum are not in scale.....18
Figure 19 Overview of chip design and behaviour....19
Figure 20 Design of the photonic chip....20

LIST OF ACRONYMS

AMF	Advanced Micro Foundry
AWG	Arbitrary Wave Generator
BER	Bit-Error-Rate
BTO	$BaTiO_3$ material
CMA-ES	Covariance Matrix Adaptation Evolution Strategy
CW	Continuous Wave
DD	Direct Detected
ESR	Early Stage Researcher
ETN	European Training Network
FM-ELM	Frequency-Multiplexed Extreme Learning Machine
FM-RC	Frequency-Multiplexing Reservoir Computer
HHI	Heinrich-Hertz-Institut
IFISC	Institute for Cross-Disciplinary Physics and Complex Systems
IM	Intensity-Modulated
MMIs	Multi-Mode Interferometers
PCB	Printed Circuit Board
POST-DIGITAL	Project 'POST-DIGITAL - European Training Network on Post-Digital Computing' EC GA 860360
SiN	Silicon-Nitride
SOA	Semiconductor Optical Amplifier
ULB	Université Libre de Bruxelles
VLC	VLC Photonics (Hitachi Group)
QAM	Quadrature-Amplitude Modulations

1 INTRODUCTION

This deliverable reports on experimental advancements of various designs for neuromorphic hardware. Contributions from ESRs at Ugent-imec, ULB, IBM, IFISC and VLC are reported. Many of these results were obtained through collaborations between ESRs and during their secondments at institutions within the POST-DIGITAL network. The deliverable is organized in individual section, each reporting on a different hardware design and its relevant results.

2 FOUR-PORT RESERVOIR CHARACTERIZATION AND EXPERIMENTAL RESULTS

This section details characterization and experimental results pertaining to an integrated photonic reservoir designed by imec-UGent, which we term the Four-Port Architecture. Since characterizations of the reservoir itself were previously reported in Deliverable 3.1, this report will only provide a high-level description of the reservoir's design which is found in Section 2.1. Next, Section 2.2 will focus on the characterization of the integrated readouts including two different weighting structures. Finally, Section 2.3 will report on the use of the reservoir in experimental setups for the equalization of high-speed telecom signals.

2.1 FOUR-PORT RESERVOIR ARCHITECTURE

The reservoir architecture used in this section is an integrated Silicon-Nitride (SiN) based photonic chip. Multi-Mode Interferometers (MMIs) are used as nodes that perform linear combinations of three inputs and redistribute them onto three outputs. Two of these inputs come from the reservoir itself, while the third input is reserved for the injection of an external signal. Similarly, two of the three outputs lead to other nodes while the third output is connected to the readout. The nodes are connected by spiraled waveguides which introduce delays between signals, allowing for meaningful mixing, as well as introduce amplitude and phase modulations on the signals.

Figure 1 shows a sample 4-node reservoir design. Note that this architecture contains only the reservoir, without any readout structure. Output signals are retrieved through grating couplers, allowing the detection of the reservoir states. Such an architecture is helpful when data collection is needed for offline training or when power losses are of concern (indeed, note that adding weighting elements and a summation tree introduce several dBs of losses).

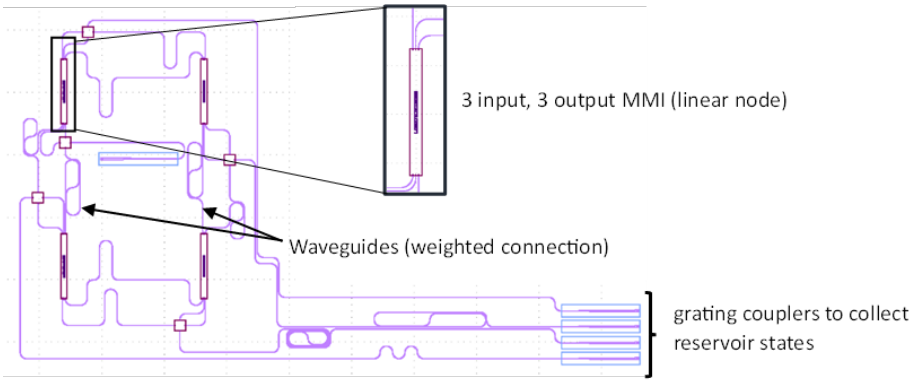

Figure 1 Design of a 4-node reservoir without an integrated readout

Figure 2 shows a 4-node reservoir with a readout structure. The weighting elements manipulate the different node signals, which are then summed and routed to a single grating coupler. Monitoring grating couplers are also available at different stages of the system. The next section will expand on the behaviour of these weights.

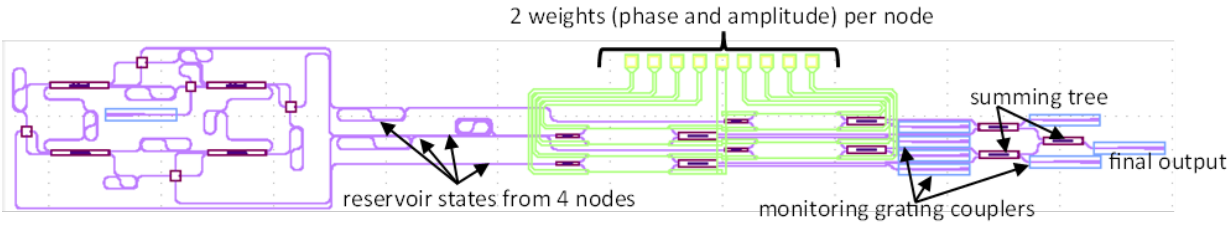

Figure 2 Design of a 4-node reservoir with integrated readout

2.2 Readout Weights

The weighting structures fabricated were either based on tungsten heaters or ferroelectric $BaTiO_3$ material (BTO). In the subsections below, characterizations of each of the two weighting techniques is detailed.

2.2.1 Tungsten Heaters Weights

The heater-based weights were characterized as part of a reservoir readout. The smallest reservoir with 4 nodes was used, which is the same one shown in Figure 2. A zoomed-in snippet of the readout is shown in Figure 3 with numbered nodes.

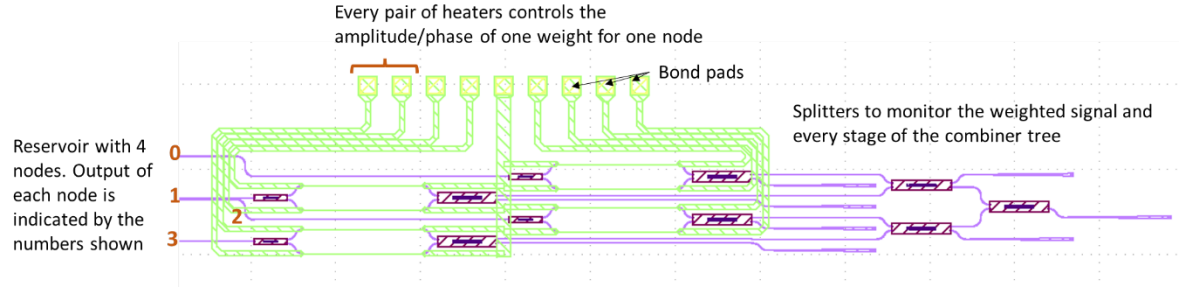

Figure 3 Readout with weights

The weights were controlled by a pair of current drivers commanded through a Python script, as shown in Figure 4a. Wiring between the current drivers and heaters was realized through wire-bonding, as shown in Figure 4b. The wire-bonding facilitates the placement of jumper wires on a printed circuit board (PCB) for connections, as opposed to the delicate process of landing pins on the chip itself.

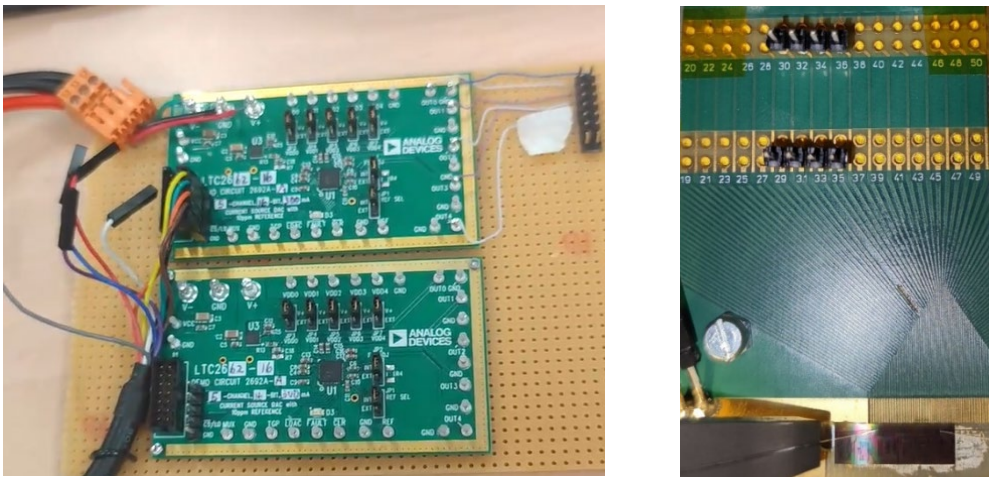

Figure 4 a. (left) Current drivers used to control readout weights b. (right) Wire-bonded chip placed on a PCB

Figure 5 shows the responses of the two heaters that belong to node 1. The transmitted powers have been measured by sweeping the current of one heater while keeping the other at 0 mA. A modulation depth of over 25 dB was measured for both heaters. Note that to achieve such modulation depth, a current sweep nup to 60 mA is required.

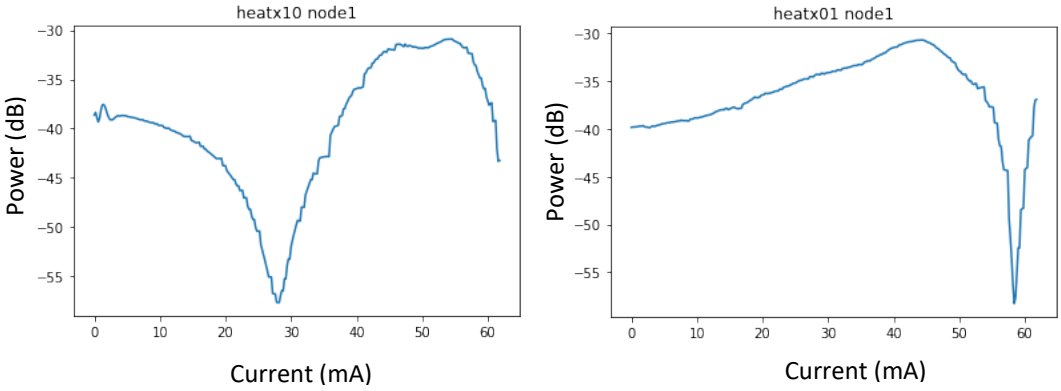

Figure 5 Current vs output power for the pair of heaters of node 1

To further characterize the weights, the pair of heaters for node 1 were driven together. This is done by performing a nested loop and the expected behaviour is seeing a shift in the power dip as the outer weight is driven. This is shown in Figure 6, where a small shift in the dip observed when the outer weight reaches 14 mA. Unfortunately, these weights were not meant for extended use and their sweeping led to the burning of the inner weight.

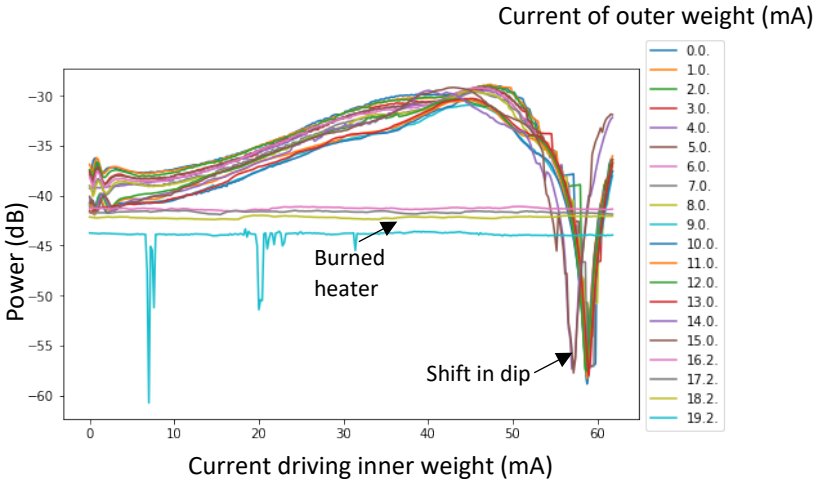

Figure 6 Dual driving of a pair of weights

The current density necessary to induce a strong modulation depth was too high for the heaters to sustain. This meant that driving them consistently near 60 mA would cause them permanent damage. As such, they cannot be used for experiments since during online training the driving current will constantly be swept to high values.

These characterizations were done by Sarah Masaad at UGent-imec.

2.2.2 BTO Weights

The BTO weights were characterized both as part of an 8-node reservoir as well as part of test structures. Similar to the wire-bonding shown in Figure 4, the chip was bonded to a PCB to facilitate the driving of weights.

The behaviour of the BTO weights is strongly dependent on the polarization of the light in the structure. This is shown in Figure 7: employing the wrong light polarization, no modulation is visible (panel a), on the other hand, employing the correct light polarization, modulation is visible (panel b).

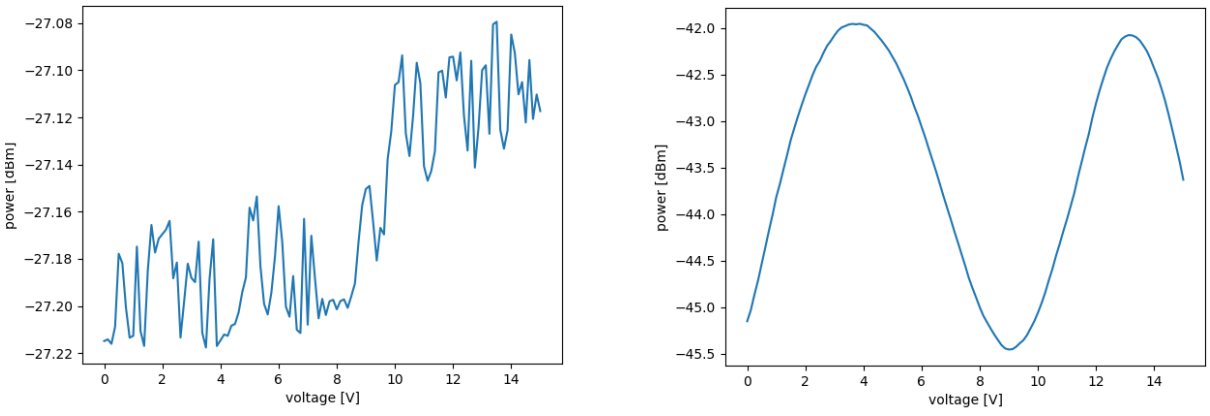

Figure 7 a. (left) no modulation due to wrong polarization of light b. (right) optimized polarization hence modulation is seen

Despite best effort to optimize polarization for the BTO weights, they exhibited high variance in modulation depths, both on the same chip and on different chips. This is shown in Figure 8, where the modulation depths of 8 weights on a single chip are shown to vary between 4 and 20 dB.

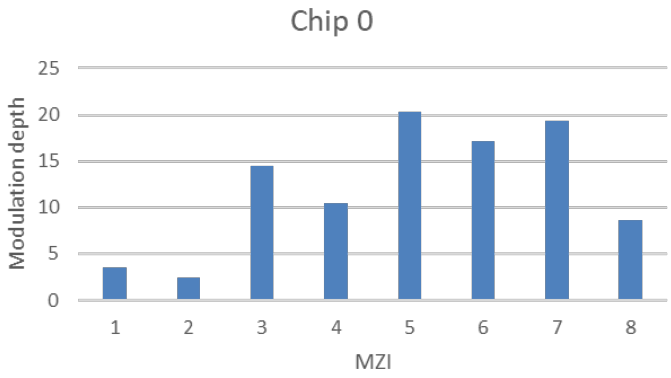

Figure 8 Modulation depths of 8 nodes on a reservoir chip

These characterizations were done at UGent in collaboration with Elger Vlieg (IBM) and Alessandro Lupo (ULB) during their secondments.

Based on the characterization results, only the BTO-based structures have been considered usable in a system experiment, which is detailed in the following section. In addition, experimental data collection on a reservoir without a readout structure is also detailed.

2.3 Telecommunication Experiments

In this section we show the use of the reservoir in an experimental setup as part of the signal processing required to equalize a distorted optical fiber signal. The first subsection details the equalization of an intensity modulated and direct detected signal. In the second subsection, coherent transmission and detection are set up with a reservoir in the pipeline.

2.3.1 Intensity-Modulated (IM) and Direct Detected (DD) Signals

An 8-node reservoir with an integrated readout deploying BTO weights was used for the online equalization of an IM/DD system. The design of the reservoir is shown in Figure 9.

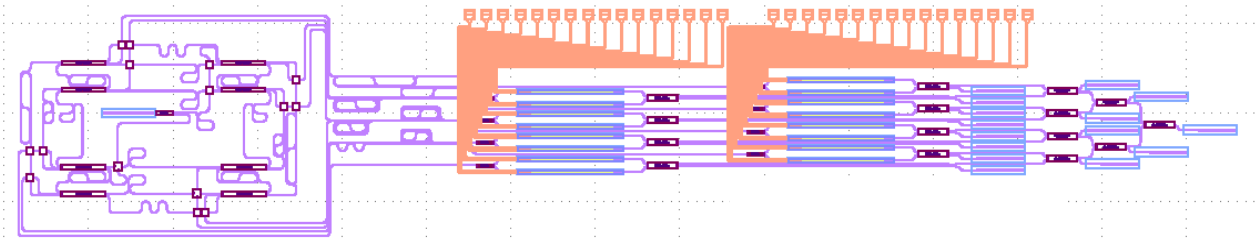

Figure 9 An 8-node reservoir with integrated BTO weights and summation tree

Despite the small size of the reservoir, significant power losses are incurred at different components. For example, the grating couplers induce around 7 dB losses per coupler and the BTO weights have an insertion loss of 4 dB per weight. Moreover, the summation tree introduces a 3 dB loss at every stage. The accumulated losses can be reduced by, e.g., replacing the grating couplers with edge couplers and using other weighting structures. However, using this architecture we expect the bit error rate results to be noise limited. This is evident from the back-to-back verification we did. In such a back-to-back setup, the transmitter (tx) and receiver (rx) are connected to each other with no fiber in between. The data recorded is shown in Figure 10a.

Then, the reservoir is introduced between the transmitter and receiver and the same data is collected and shown in Figure 10b. The deterioration in signal-to-noise ratio is visually evident from the 0-bit header.

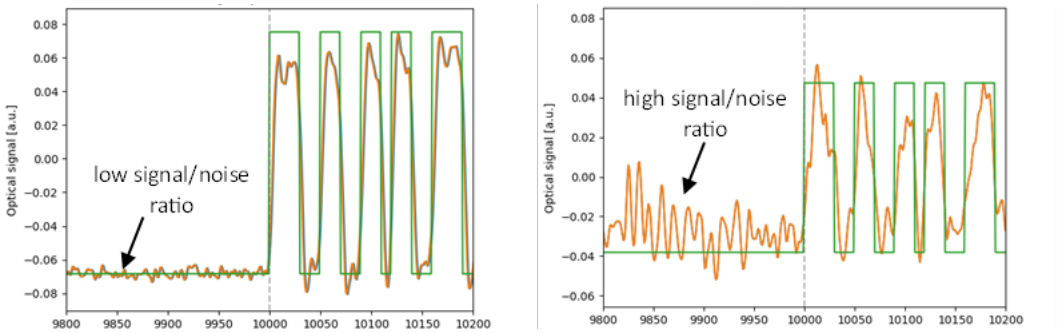

Figure 10 a. (left) data from tx-rx setup b. (right) data from tx-reservoir-rx setup

Figure 11 shows the setup built to perform this experiment. A 25 km fiber was used to induce dispersion on an IM signal modulated at a rate of 28 Gbits/second. To introduce nonlinear errors originating from self-phase modulation, the power launched into the fiber was 15 dBm. The signal was passed into the reservoir for equalization, which required adjusting the reservoir weights to achieve a low bit-error-rate (BER). The weights were adjusted automatically based on an online training algorithm that attempts to match the received signal to the target signal. The received signal is the combined and detected output from the reservoir, while the target signal is the transmitted bit stream.

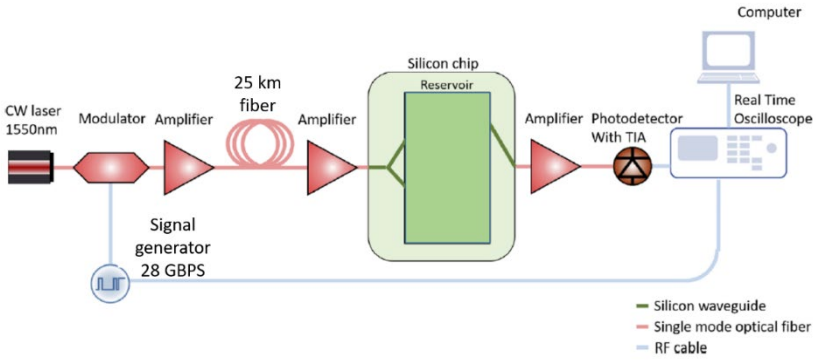

Figure 11 IM/DD system with a distorting optical fiber and a reservoir for equalization

Since high losses are incurred in the reservoir, a pair of amplifiers is used before and after the reservoir to maximize the detected power. Furthermore, as a preliminary step in the reservoir training, the weights are optimized to maximize transmission or, in other words, minimize the power losses. This is shown in Figure 12a. In the next step, the weights are optimized to reduce the bit error rate as shown in Figure 12b.

The training algorithm used is known as the covariance matrix adaptation evolution strategy (CMA-ES). This is an evolutionary black-box optimization algorithm commonly employed in neural network hyperparameter tuning. CMA-ES consists of searching for the optimal set of weights by sampling their values from a multivariate Gaussian distribution. In each epoch, the distribution parameters (mean and covariance) are updated based on the achieved performance. This is useful for online training since no derivatives or backpropagation is required, which are computationally demanding and challenging to implement in physical systems.

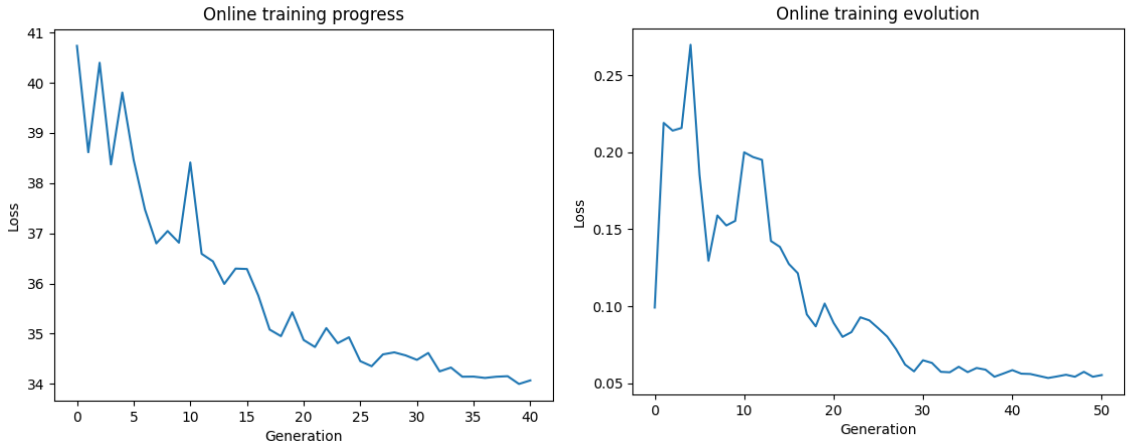

Figure 12 a. (left) preliminary optimization to maximize transmission b. (right) optimization to minimize bit error rate

Through this process, the BER was reduced from 0.15 to 0.05. Note that the starting BER show in Fig 12b is 0.1 since the preliminary optimization step of increasing the transmission caused an improvement in BER from 0.15 to 0.1.

Unfortunately, further reductions in BER were not achievable due to limitations in the experimental setup. To start with, the reservoir size of 8 nodes was smaller than the standard size used in similar offline-training experiments as reported in [1]. Furthermore, due to the high losses on chip, the BER was heavily influenced by the signal-to-noise ratio limitations. Finally, as reported in the previous section, the modulation depths from the BTO weights varied and some of them were very low. This affected the programmability of the weights and thus limited the achievability of low BER. Nonetheless, these results constitute strong foundations for complete on-chip equalization of an optical transmission system.

Results of this experiment were obtained at UGent in collaboration with Elger Vlieg (IBM) and Alessandro Lupo (ULB) during their secondments.

2.3.2 Coherently Modulated and Coherently Detected Signals

In this section, we detail the experimental data collection of coherently modulated signals through the reservoir. In this experiment, a 16-node reservoir without an integrated readout is used. The experiment was conducted at Aston university during Sarah Masaad's secondment. The setup built is shown in the figure below.

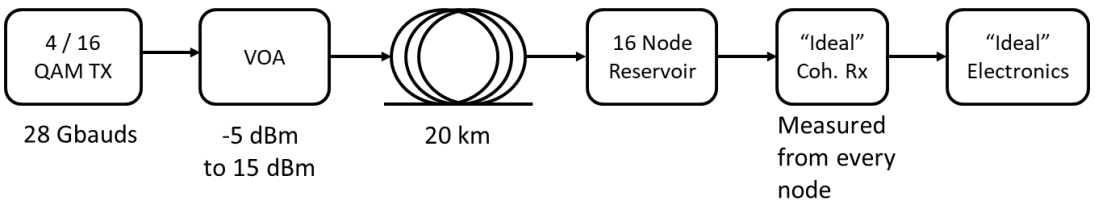

Figure 13 Coherent transmission setup

Two modulation formats, namely 4 and 16 Quadrature-Amplitude Modulations (QAM) were used. The power sent into the fiber was swept between -5 and 15 dBm. This was done to induce a variation of linear and nonlinear errors.

The data right after the fiber was coherently detected, as well as the data through the reservoir, whereby every state of the reservoir (from every node) was recorded. We opted for a reservoir with no integrated readout since the system with a readout was very lossy and using the integrated readout would have been very challenging. In addition, the setup suffered from constant drifts and needed frequent realignment, which meant it was better to collect data and then process it offline. Furthermore, the largest available reservoir with integrated readout was an 8-node one, which would be too small for such a task.

This data will serve as a stepping stone to understand what kind of nonlinearity is required for such data, since their offline processing allows us to investigate different hyper-parameters without worrying about the lab environment changes. Although results were not yet achieved from this data set, the thorough data collection done during the secondment at Aston will allow a detailed investigation of experimentally collected data. Since results were coherently collected from every node of the reservoir, the complete amplitude and phase information is available, which allows doing the training on the reservoir states offline. This study will then facilitate training on a new version of chips customized for coherent receivers.

[1] S. Sackesyn, C. Ma, J. Dambre, and P. Bienstman, “Experimental realization of integrated photonic reservoir computing for nonlinear fiber distortion compensation,” Optics Express (2021)

3 CHARACTERIZATION OF READOUT LAYER FOR FREQUENCY-MULTIPLEXING COMPUTERS

This section reports the progress of the development of an integrated optical readout layer designed for a frequency-multiplexing optical computer. At ULB, two frequency-multiplexing schemes for optical information processing have been developed. The first scheme is a frequency-multiplexing reservoir computer (FM-RC) while the second is a frequency-multiplexed extreme learning machine (FM-ELM). While the FM-RC constitutes a recursive neural network able to process time series, the FM-ELM constitutes a memoryless feed-forward neural network able to perform classification and regression tasks. Both schemes have been successfully demonstrated in optical-fiber setups [1, 2].

The proposed integrated readout layer consists of two parts. The first part is a programmable spectral filter, able to apply independent attenuations on different wavelength regions of the light spectrum. The second part is a wavelength converter based on the saturation of gain of a semiconductor optical amplifier (SOA). The working principle of the readout layer is the following. The reservoir state (in the FM-RC case), or the hidden layer state (in the FM-ELM case), is encoded in a frequency comb, each line representing the signal of a neuron. The programmable spectral filter applies weights on the neuron signals, by attenuating each wavelength by the amount corresponding to the desired weight. The output of the spectral filter is still a frequency comb, whose lines have been attenuated according to the output weights. The weighted comb is then injected in the SOA-based wavelength converter, where the overall comb power, i.e. the weighted sum of neuron signals, is transferred on a new wavelength, thus generating an optical output on a single wavelength.

In the following, we provide a detailed description and characterization of the readout layer. Details about the programmable spectral filter are reported in Section 3.1, and details about the wavelength converter are reported in Section 3.2.

3.1 PROGRAMMABLE SPECTRAL FILTER

3.1.1 Design

The frequency-multiplexing computer is based on a frequency comb whose lines encode neuron signals. In the current experiments, the comb is located in the C-band, centered around 1550 nm, and the spacing between consecutive lines is approximately 20 GHz. The spectral filter is designed to be compatible with these specifications. We note an important detail: our frequency-multiplexing scheme allows to fine-tune the center of the frequency comb. Thus, it is not necessary to deploy tuning mechanisms in the filter, as the frequency comb center can be tuned to match the filter transfer function (i.e., the comb central wavelength can be chosen in such a way to center the comb lines to the channels of the filter). The current design allows to independently attenuate 16 comb lines.

The programmable spectral filter is schematized in Figure 14(a). The design is composed of three stages. First, a wavelength de-multiplexer stage separates each channel; second, an attenuation stage, composed of 16 individually addressable attenuators, weight each comb line; third, a wavelength multiplexer stage, symmetric to the de-multiplexer, recombines the signals into a single output channel.

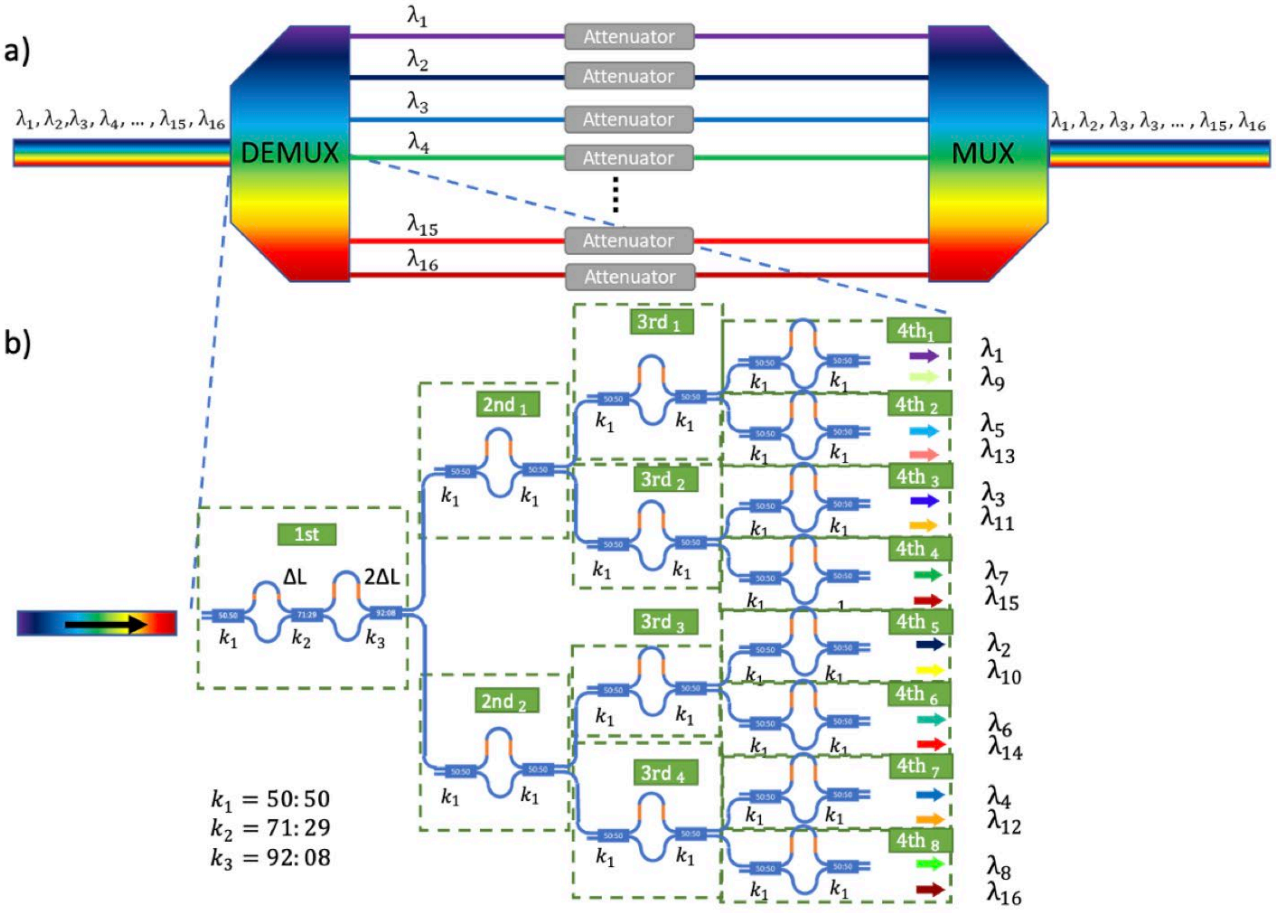

Figure 14 (a) Conceptual scheme of the programmable spectral filter. From left to right: 1-to-16 wavelength de-multiplexer, array of 16 attenuators, 16-to-1 multiplexer. (b) Detail of the de-multiplexer architecture. The de-multiplexer is composed of 15 lattice filters organized in a 4-stage binary three.

Figure 1(b) reports in details the layout of the 1-to-16 channels wavelength de-multiplexer. The de-multiplexer consists of 15 lattice filters organized in a 4-stage binary tree. In general, a 1-to-N de-multiplexer would be

composed of N − 1 lattice filters organized in log2(N) stages. The 16-to-1 channel multiplexer (not represented here) is obtained by just mirroring the design of the de-multiplexer. All the filters, excluding the ones in the first stage, are constituted by two multimode interference couplers (MMI) and an optical delay line. The lattice filter in the first stage has the biggest influence on the (de)multiplexing performance, hence it is realized by a more complex design which involves three MMIs and two optical delay lines and assures a flatter transfer function. The MMI splitting ratios and the delay line lenghts are chosen to achieve the desired (de)multiplexing function [3].

The attenuation stage is composed of 16 Mach-Zehnder modulators based on thermo-optical phase shifters. The heating elements are positioned in a “zig-zag” fashion to minimize the thermal cross-talk.

The filter chip has been fabricated by Advanced Micro Foundry (AMF) in a multi-project wafer run on a silicon-on-insulator platform. Concerning possible alternative integration platforms, we note that Indium Phosphide (InP) is not an easily-viable option, as the minimum bending radius for waveguides is high and would severely increase the space occupation of the long delay lines.

3.1.2 Characterization

The experimental setup for the characterization of the chip is depicted in Figure 15. Optical connections are realized by a fiber-array, while electrical connections are realized by a multi-contact probe. The characterization consists of measuring the transmission spectrum while sweeping the attenuations. Attenuations are swept by changing the heater currents in the range 0-5 mA. This method allows to measure insertion losses (i.e., the minimum attenuation possible), extinction ratios (i.e., the maximum attenuation possible) and cross-talks (i.e. the response of one channel when another channel is addressed). Results of the characterization are reported in Figure 16. The average measured insertion loss is 12.5 dB; the average measured extinction ratio is 14.9 dB; the average measured cross-talk is 0.57 dB.

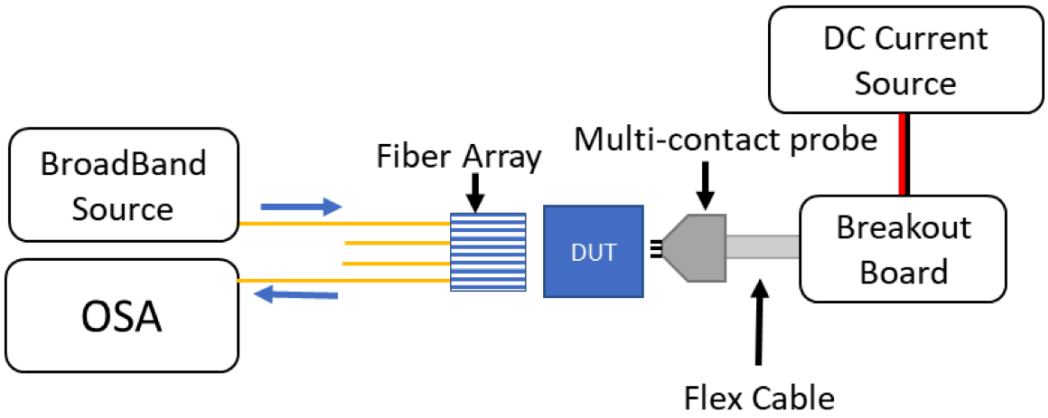

Figure 15 Experimental characterization setup. OSA: optical spectrum analyser; DUT: device under test.

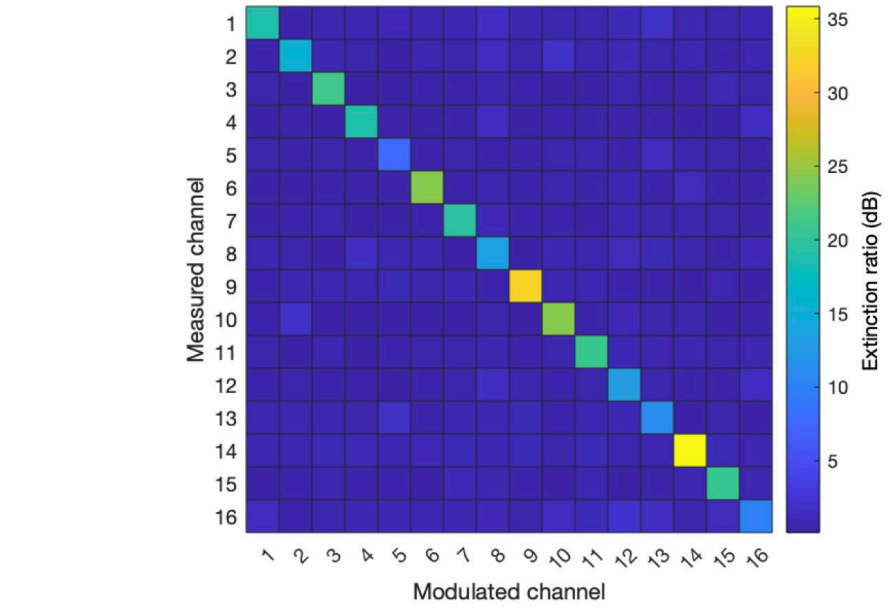

(a)

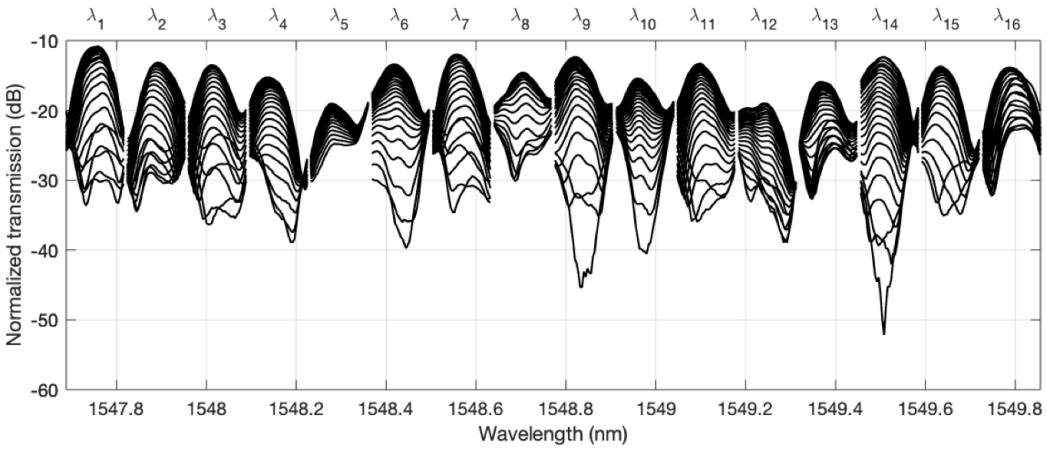

(b)

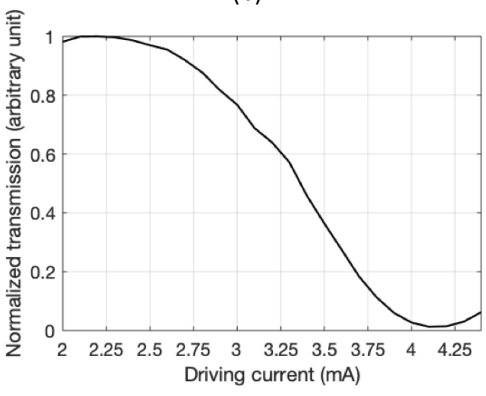

(c)

Figure 16 (a) Cross-talk map of the spectral filter. The map reports the maximum extinction ratio measured on the "measured channel" when the "modulated channel" attenuation is swept. In-diagonal elements represent the actual extinction ratio of every channel, while the off-diagonal elements represent the cross-talk. The average cross-talk is 0.57 dB. (b) Measured transfer function for each of the 16 channels for different values of the driving current (in the range 0-5 mA). (c) Example of transmission function of a single channel.

3.2 Wavelength Converter

The design of the SOA-based wavelength converter is depicted in Figure 17. Both a frequency comb (encoding neuron signals in its lines) and a (low-power) probe signal are injected in a SOA. The SOA gain is saturated by the comb power (i.e., by the sum of the powers of neuron signals). The saturation affects the gain experienced by the probe. Thus, after passing through the SOA, the probe signal acquires a modulation dependent on the sum of neuron signals. A bandpass filter discards the comb and transmits only the modulated probe. This scheme allows to perform optical summation of the neuron signals without electro-optical conversions.

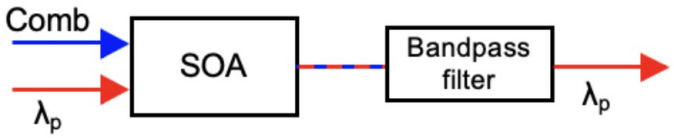

Figure 17 Scheme of the SOA-based wavelength converter. Both a frequency comb (blue arrow) and a low-power probe signal (λ_p, red arrow) are injected in the SOA. The SOA gain is saturated by the comb power and the saturation affects the gain experienced by the probe signal. A bandpass filter selects only the probe signal, whose power depends on the sum of the powers of the comb lines.

The SOA-based wavelength converter chip has been fabricated by the Heinrich-Hertz-Institut (HHI), in a multi-project wafer run on a InP platform. Due to delays in fabrication, the chip is currently being characterized and will be employed for reservoir computing benchmarks at ULB by the ESRs Alessandro Lupo and Tigers Jonuzi even after the conclusion of the POST-DIGITAL project.

The envisioned application of this chip is represented in Figure 18 and reported in [4]. The frequency comb encoding neuron values to be weighted is supplied to two filters. The first filter applies positive weights and blocks the lines that need negative weights; inversely, the second filter applies negative weights and blocks the lines that need positive weights. The two weighted combs are then supplied to two wavelength converters, thus the content of their neurons is summed and transferred to the probe wavelength λ_p. The two signals at wavelength λ_p are then made to interfere destructively. The residual comb radiation is removed through a bandpass filter. The output of the system is a signal at probe wavelength proportional to the weighted sum of neuron signals.

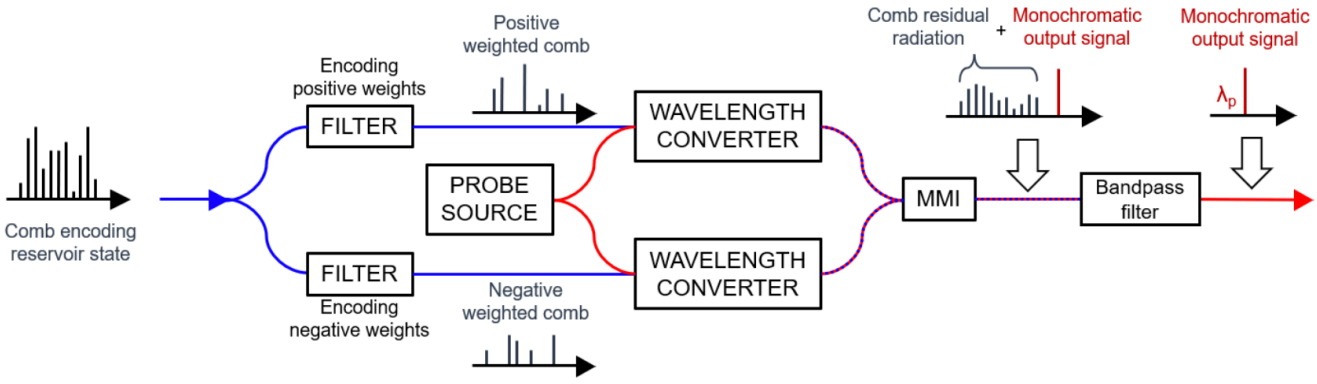

Figure 18 Envisioned application of the SOA-based wavelength converter. Note that the probe radiation power is lower than the comb power, hence the representations of the spectrum are not in scale.

[1] Butschek, L., Akrout, A., Dimitriadou, E., Lupo, A., Haelterman, M., & Massar, S. (2022). Photonic reservoir computer based on frequency multiplexing. Optics Letters, 47(4), 782-785.

[2] Lupo, A., Butschek, L., & Massar, S. (2021). Photonic extreme learning machine based on frequency multiplexing. Optics express, 29(18), 28257-28276.

[3] Jonuzi, T., Lupo, A., Soriano, M. C., Massar, S., & Domenéch, J. D. (2023). Integrated programmable spectral filter for frequency-multiplexed neuromorphic computers. Optics Express, 31(12), 19255-19265.

[4] Jonuzi, T., Lupo, A., Soriano, M. C., Gomez, J. D. D., & Massar, S. (2023). Integrated optical output layer for a reservoir computer based on frequency multiplexing. In AI and Optical Data Sciences IV (Vol. 12438, pp. 85-91). SPIE.

4 PHOTOREFRACTIVE CROSSBAR ARRAY

Artificial intelligence and the underlying neural network models are generating an unsustainable compute demand. Specifically, the synaptic signal transfer between fully connected neuron layers is computationally expensive. The synaptic signal transfer can be accelerated efficiently by the analog crossbar array compute architecture. Conceptually, the analog crossbar array is a direct hardware implementation of the synaptic interconnect layer.

Elger at IBM is developing a photonic crossbar array that exploits the photorefractive effect. This approach is particularly desirable since it supports backpropagation training and shows favourable scaling compared to other photonic approaches by leveraging holographic storage of the synaptic weights [1].

In terms of the development of the photorefractive crossbar array, we have successfully experimentally demonstrated the basic physical mechanisms and core building blocks (please see the figure below). This encompasses: the fabrication of photorefractive integrated photonic circuits, the realization of a slab waveguide routing device, and the demonstration of the writing of photorefractive synapses.

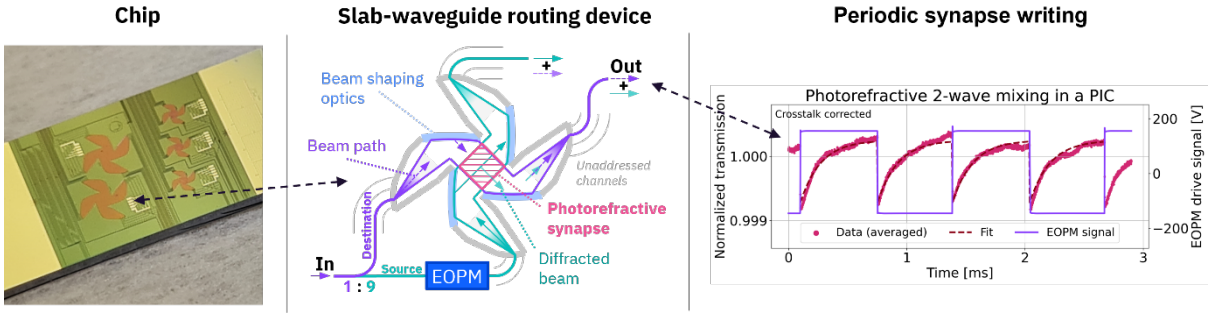

Figure 19 Overview of chip design and behaviour

[1] E. Vlieg, L. Talandier, R. Dangel, F. Horst, and B. Offrein, “An Integrated Photorefractive Analog Matrix-Vector Multiplier for Machine Learning,” Applied Sciences (2022)

5 CHARACTERIZATION OF CONVOLUTION NEURAL NETWORK ON SILICON PHOTONIC INTEGRATED CHIP

The characterization of a convolutional accelerator embedded within a silicon photonic integrated chip is reported in this section. These characterizations were carried out by Lucas Talandier (IFISC) and Tigers Jonuzi (VLC) at the Nonlinear Photonics Lab at IFISC during the latter's secondment.

For the purpose of characterizing this photonic chip, a 92GSa/s@32GHz AWG was employed to channel the test signal into the chip. A CW source, specifically a semiconductor laser, underwent modulation by a 40GHz Mach Zehnder modulator. This laser's temperature was controlled, to optimize the input wavelength. Post this, the signal was subjected to polarization control and subsequently injected into various integrated fiber couplers via a fiber array. The chip's temperature was maintained using a Peltier thermoelectric cooler. The different phase shifters were controlled by a multi-current source. All the elements of the setup were automatized, and controllable by Python/MATLAB interface.

The main objective was to validate the photonic integrated network's ability to produce the desired output kernel. This network is composed of multiple phase shifters and Mach Zehnder modulators (Figure 2), all of which rely on thermal phase shifters (with 18 embedded within the chip). Each individual phase shifter's operation induced crosstalk by heating adjacent waveguides. This phenomenon posed a significant challenge during the experiment. Another encounter was the rather short delays separating each adjacent paths (33ps) compared to the speed limits of the AWG and Mach Zehnder modulator. To ensure no crosstalk between the path, the duration of the pulse was constrained to 1 or 2 samples at 85.333Gsa/s thus superior to the bandwidth of the AWG (32GHz) and at the limit of the modulator bandwidth (40GHz @-3dB). The experiment's final outcome was a successful demonstration of kernel generation with weight optimization. This was achieved through various combinations of the operational states of the different phase modulators and phase shifters, laying a robust foundation for potential tasks like image classification.

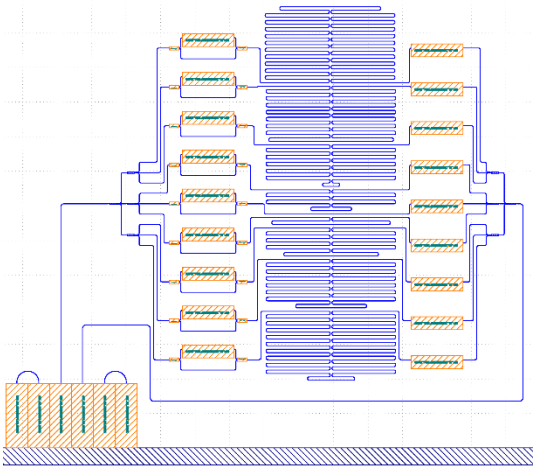

Figure 20 Design of the photonic chip